Supplementary materials for : Characteristics of tropospheric ozone depletion events in the Arctic spring: Analysis of the ARCTAS, ARCPAC, and ARCIONS measurements

J.-H. Koo, Y. Wang, T. P. Kurosu, K. Chance, A. Rozanov, A. Richter, S. J. Oltmans, A. M. Thompson, J. W. Hair, M. A. Fenn, A. J. Weinheimer, T. B. Ryerson, S. Solberg, L. G. Huey, J. Liao, J. E. Dibb, J. A. Newman, J. B. Nowak, R. B. Pierce, M. Natarajan, and J. Al-saadi

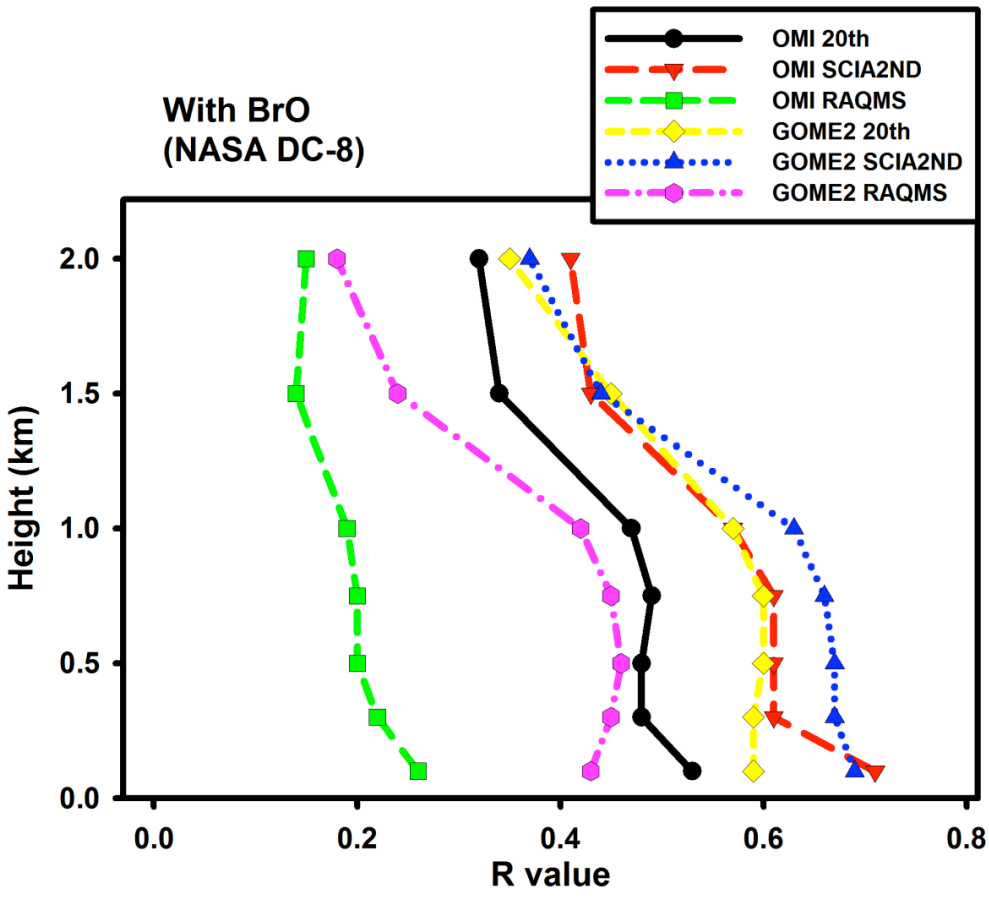

Fig. S1. Vertical profiles of correlation coefficients (R values) of retrieved tropospheric BrO columns with BrO measured from DC-8 Flights 9 and 10 (April 16 and 17). To correlate with tropospheric BrO columns with sufficient in situ data points, we integrate in situ aircraft observations of BrO, Br_2+HOBr, and soluble bromide from the surface to 7 altitude levels (100, 300, 500, 750, 1000, 1500, and 2000 m). Tropospheric column BrO measurements corresponding to the in situ data points were sampled along the flight tracks. WP-3D data were not used because no significant correlation was found with column BrO; the reason is unclear. We used six tropospheric BrO VCD products, which are OMI-20th (black), OMI-SCIA2ND (red), OMI-RAQMS (green), GOME2-20th (yellow), GOME2-SCIA2ND (blue), and GOME2-RAQMS (purple).

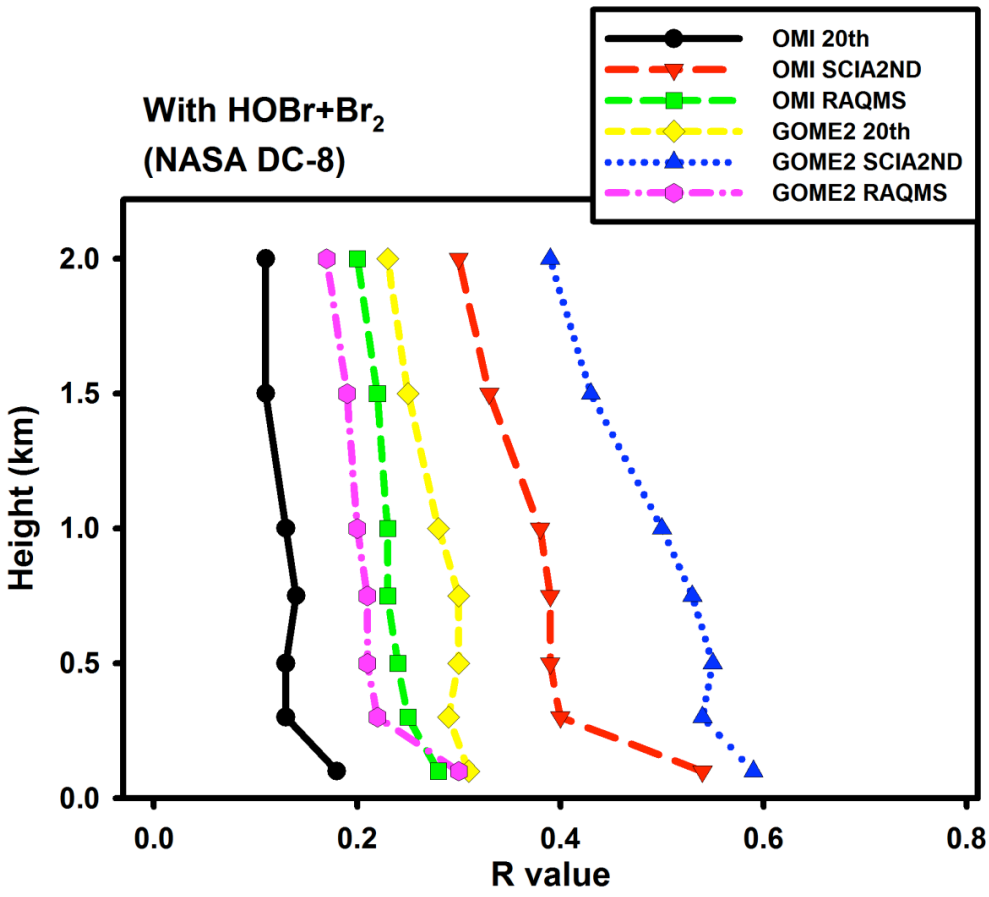

Fig. S2. Same as Fig. S1, but for correlations with integrated Br_2+HOBr in DC-8 flights (April 4, 5, 8, 9, 12, 16, and 17).

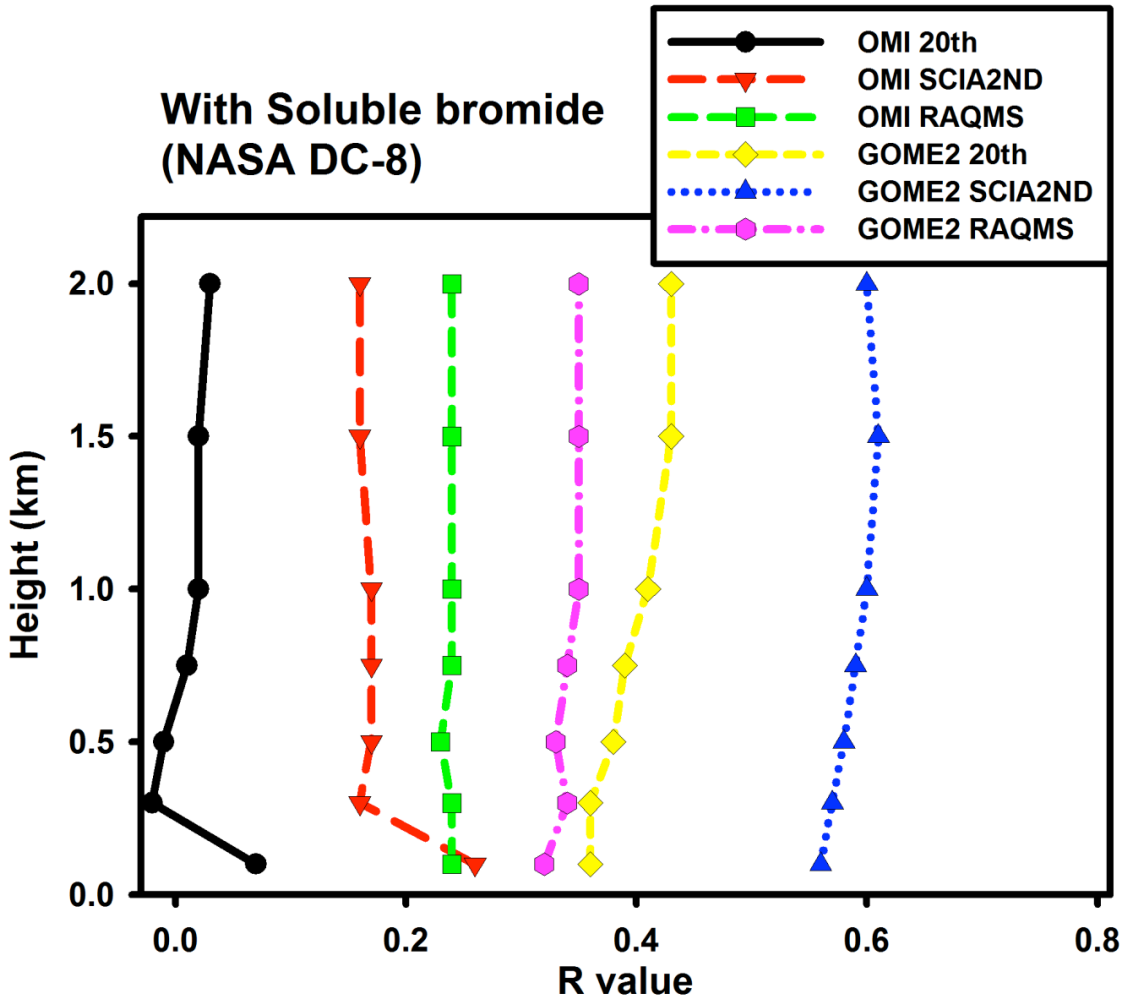

Fig. S3. Same as Fig. S2, but for correlations with integrated soluble bromide measured in DC-8 flights.

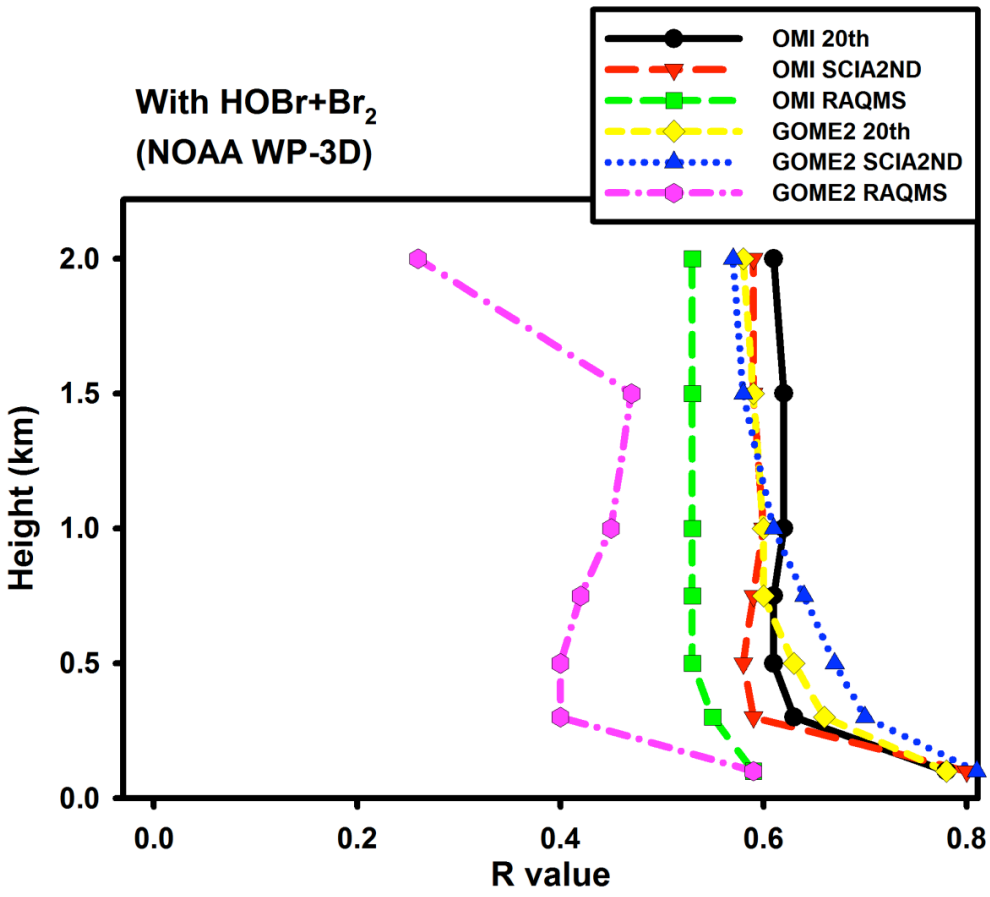

Fig. S4. Same as Fig. S1, but for correlations with integrated Br_2+HOBr in WP-3D flights (on April 12, 15, 18, 19, and 21). The more consistent correlation with Br_2+HOBr measurements during ARCPAC than ARCTAS (Fig. S2) reflects in part a smaller sampling region by WP-3D (to be shown in Fig. 5). The smaller sampling region leads to a smaller variation of the estimated stratospheric column BrO during ARCPAC than ARCTAS. The variation of tropospheric column BrO is therefore more consistent among the different products during ARCPAC than ARCTAS.

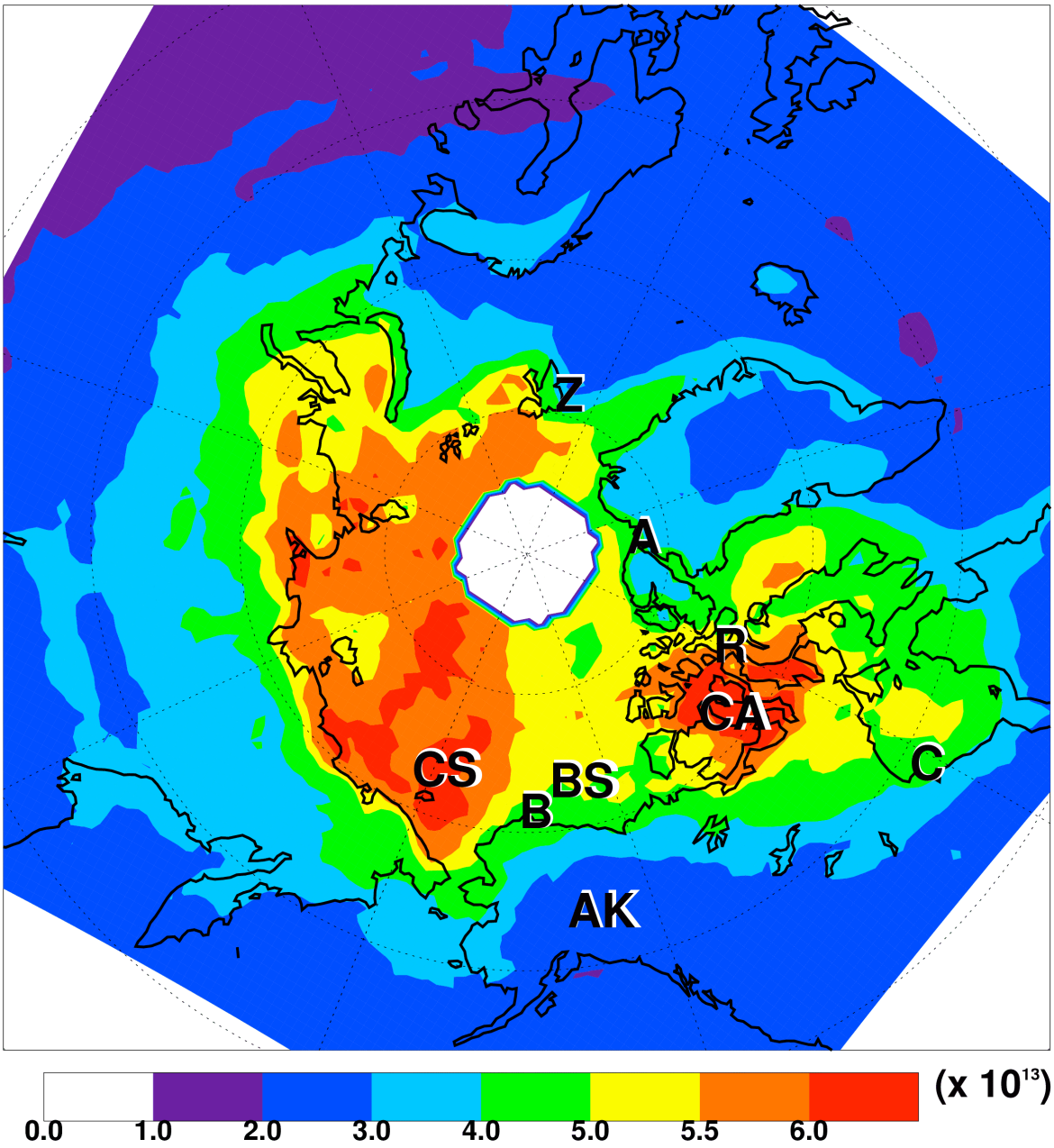

Fig. S5. Same as Fig. 2a, but for tropospheric BrO VCDs of OMI-SCIA2ND.

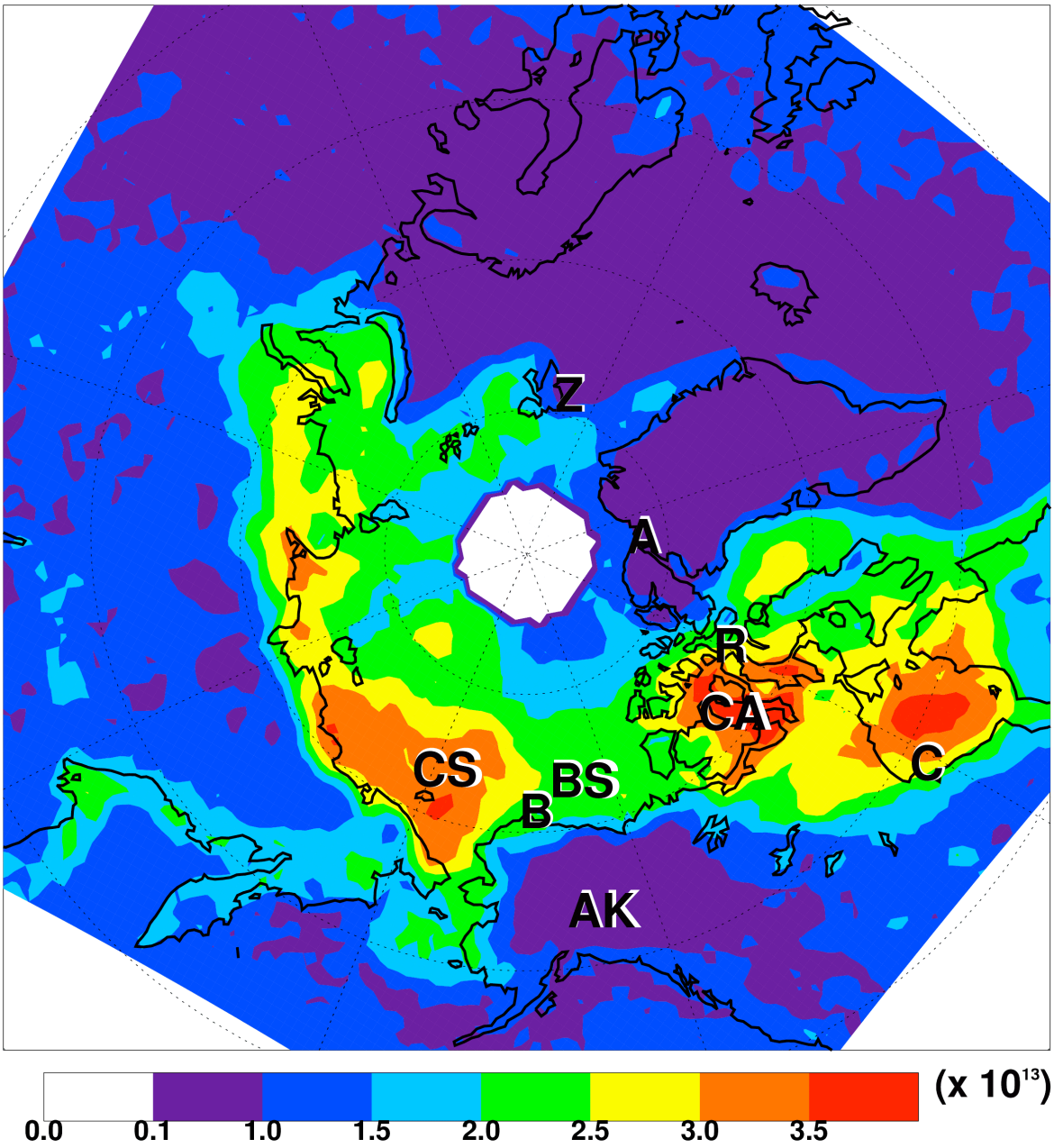

Fig. S6. Same as Fig. 2a, but for tropospheric BrO VCDs of GOME2-20th.

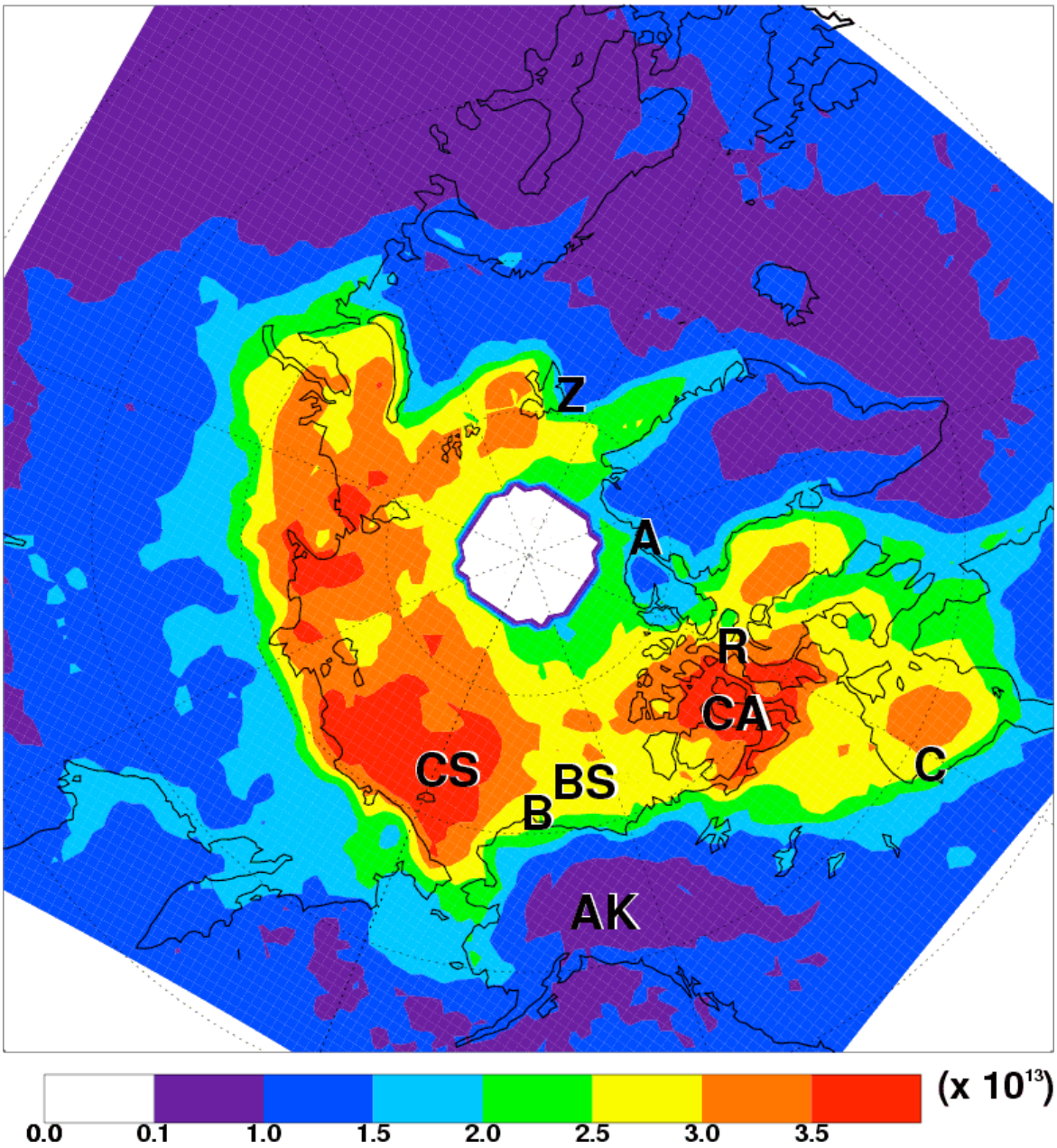

Fig. S7. Same as Fig. 2a, but for tropospheric BrO VCDs of OMI-20th.

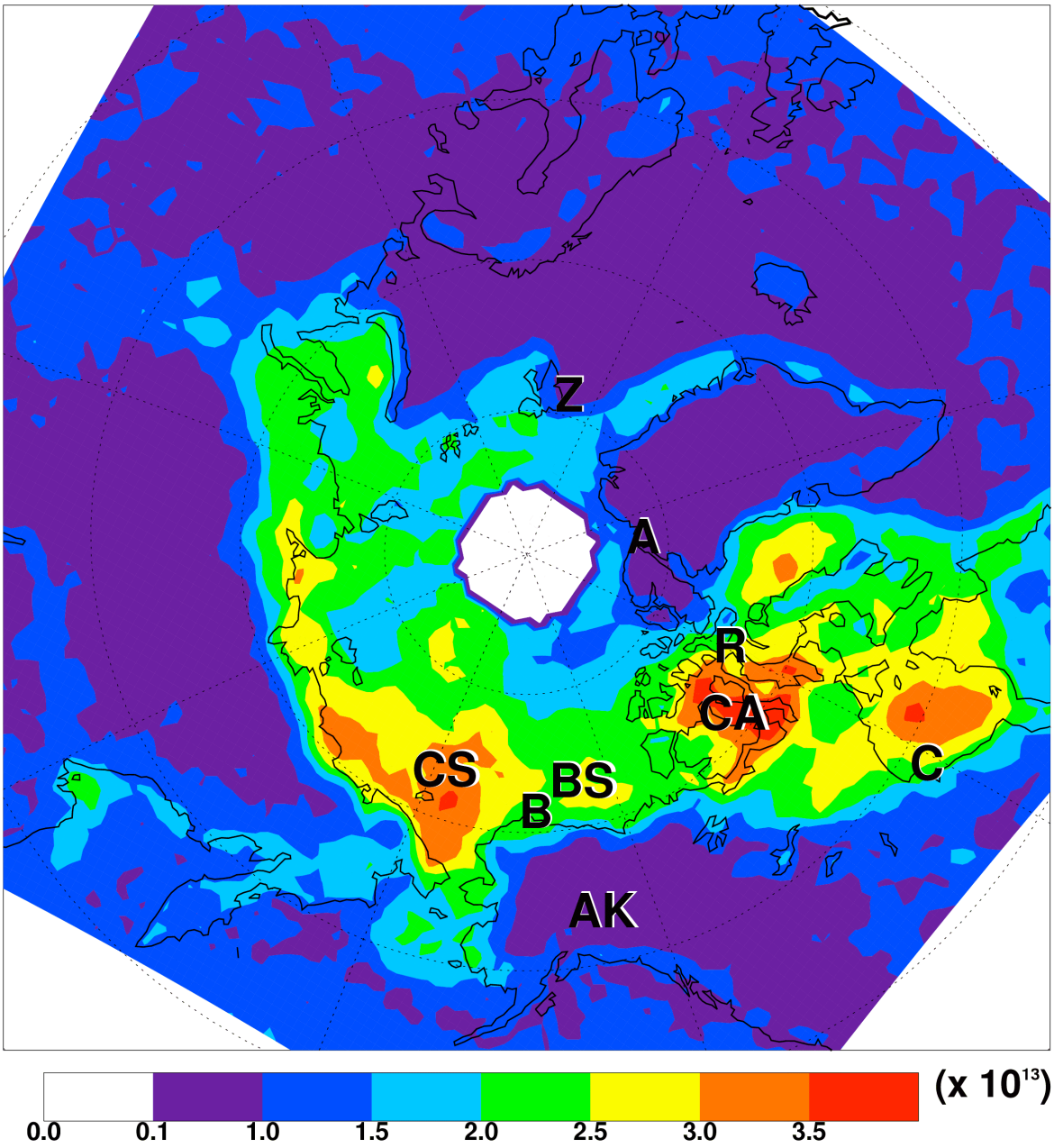

Fig. S8. Same as Fig. 2a, but for tropospheric BrO VCDs of GOME2-RAQMS.

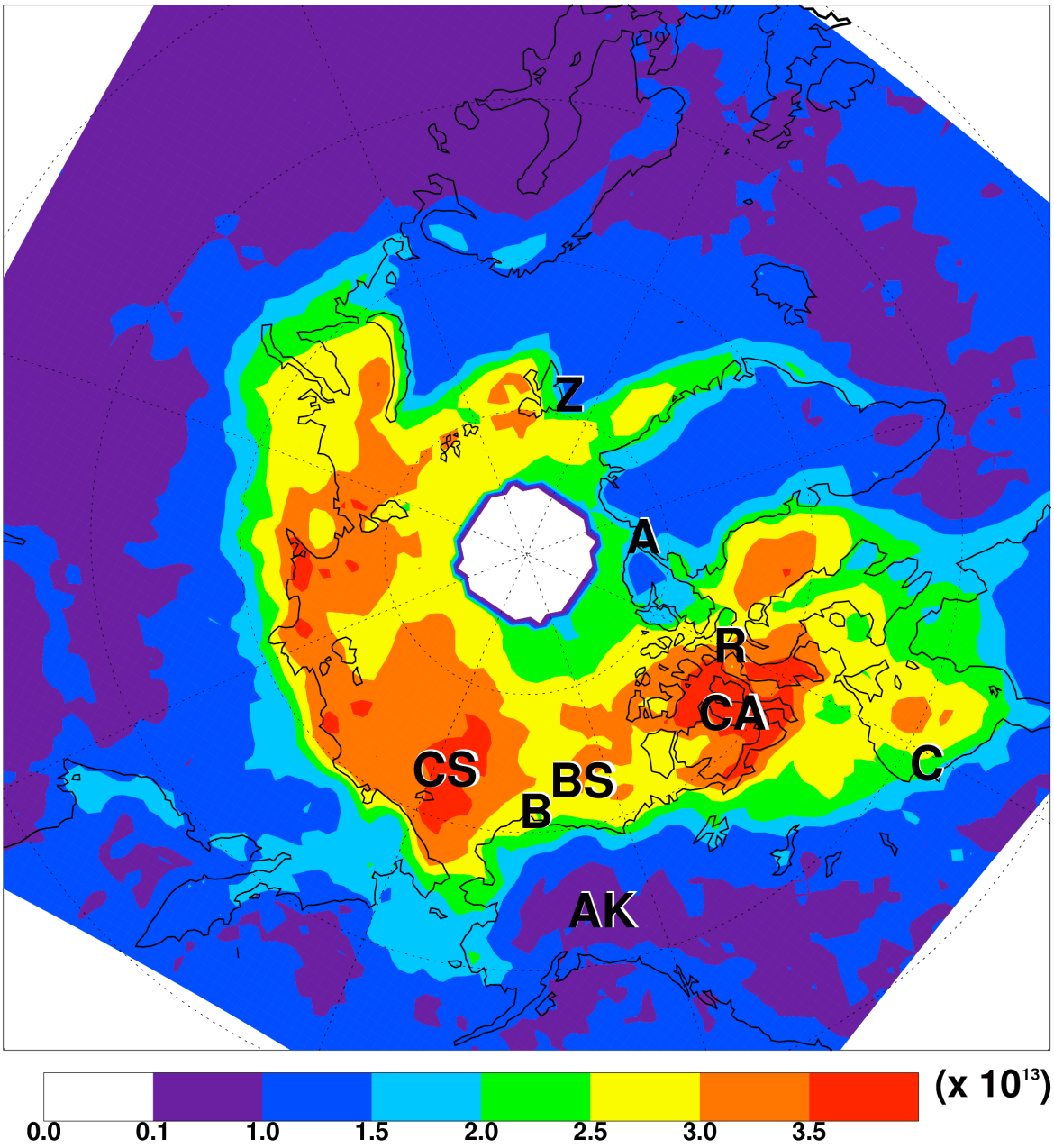

Fig. S9. Same as Fig. 2a, but for tropospheric BrO VCDs of OMI-RAQMS.

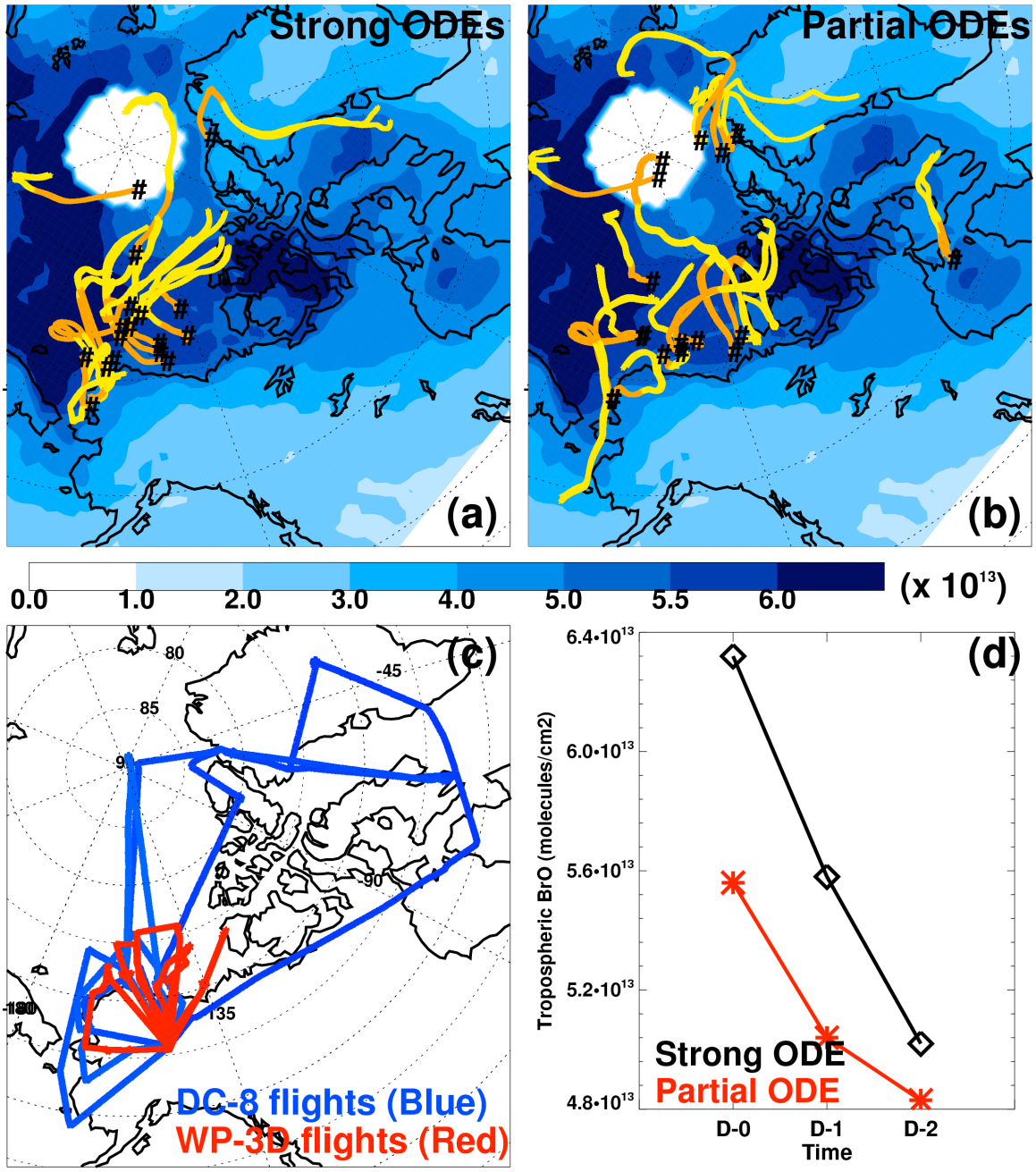

Fig. S10. Same as Fig. 5, for tropospheric BrO VCDs of OMI-SCIA2ND.

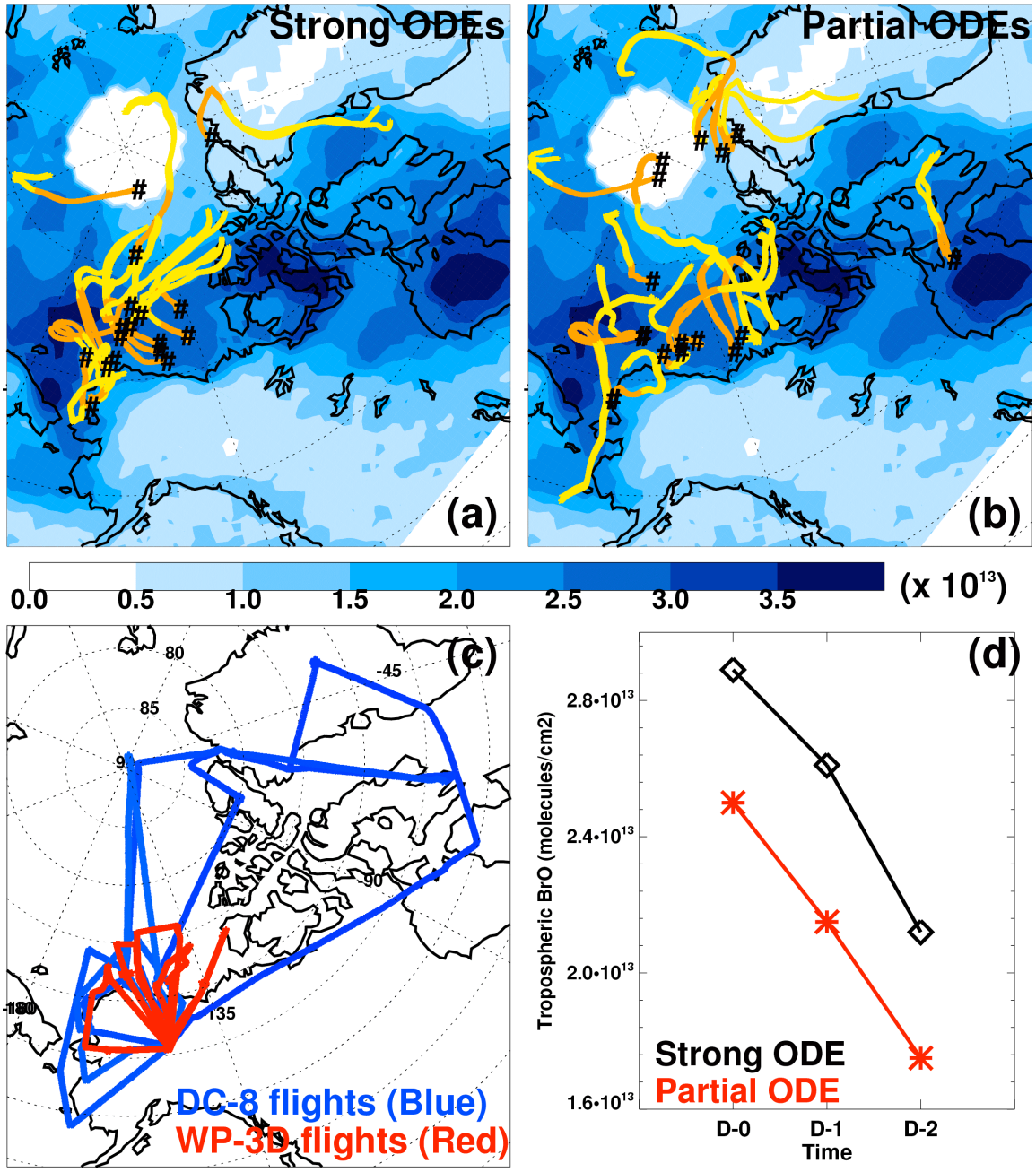

Fig. S11. Same as Fig. 5, but for tropospheric BrO VCDs of GOME2-20th.

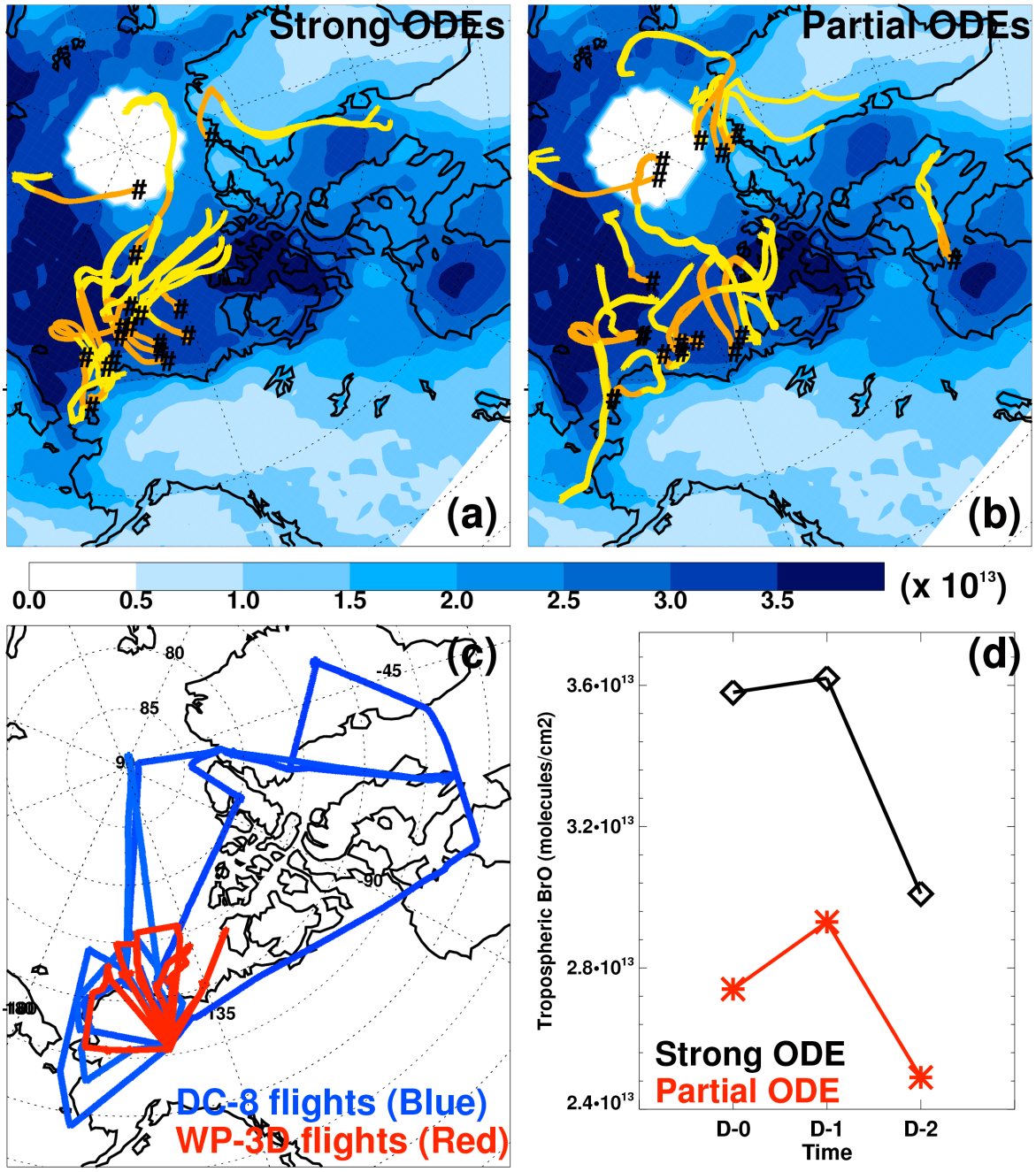

Fig. S12. Same as Fig. 5, but for tropospheric BrO VCDs of OMI-20th.

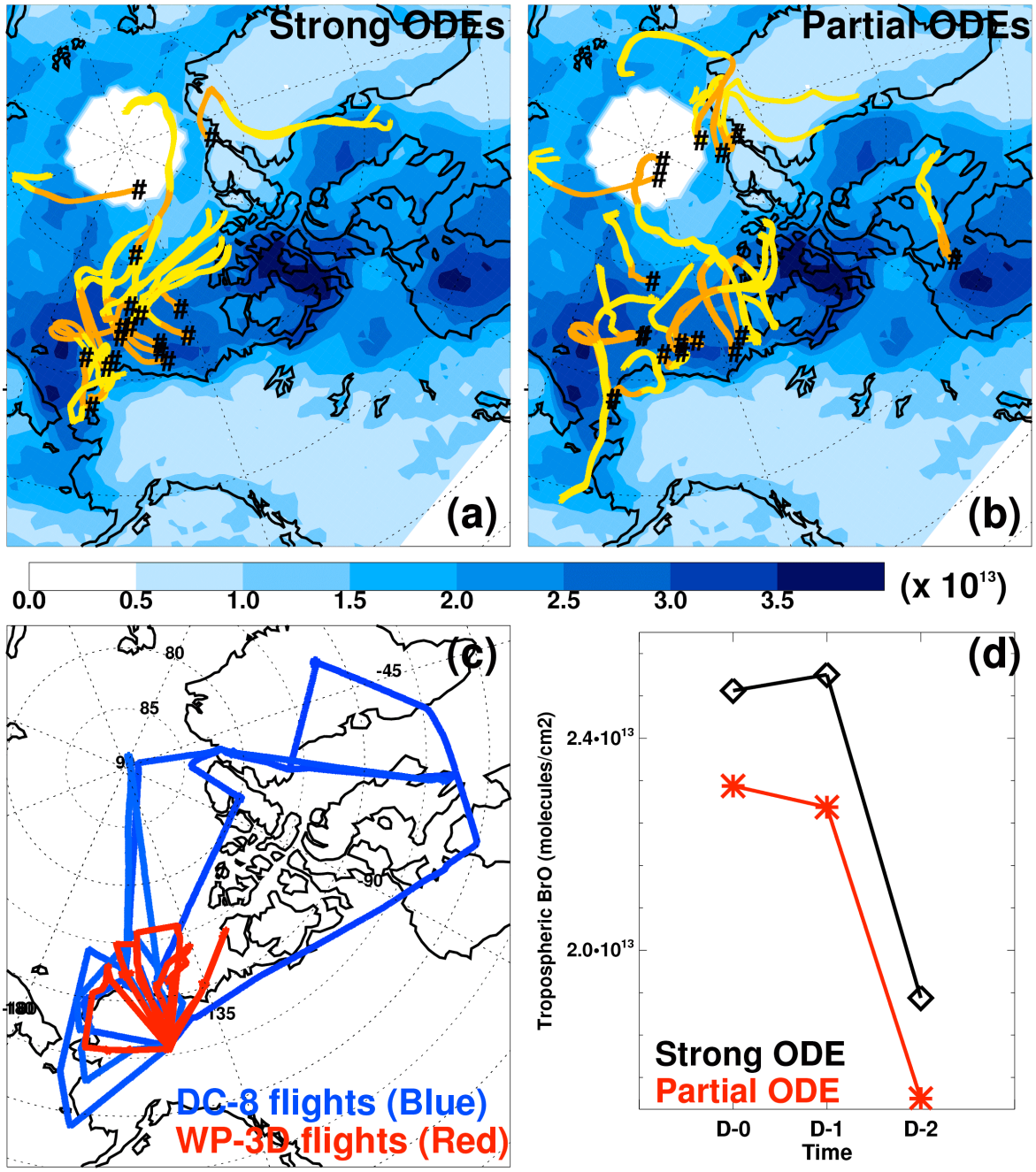

Fig. S13. Same as Fig. 5, but for tropospheric BrO VCDs of GOME2-RAQMS.

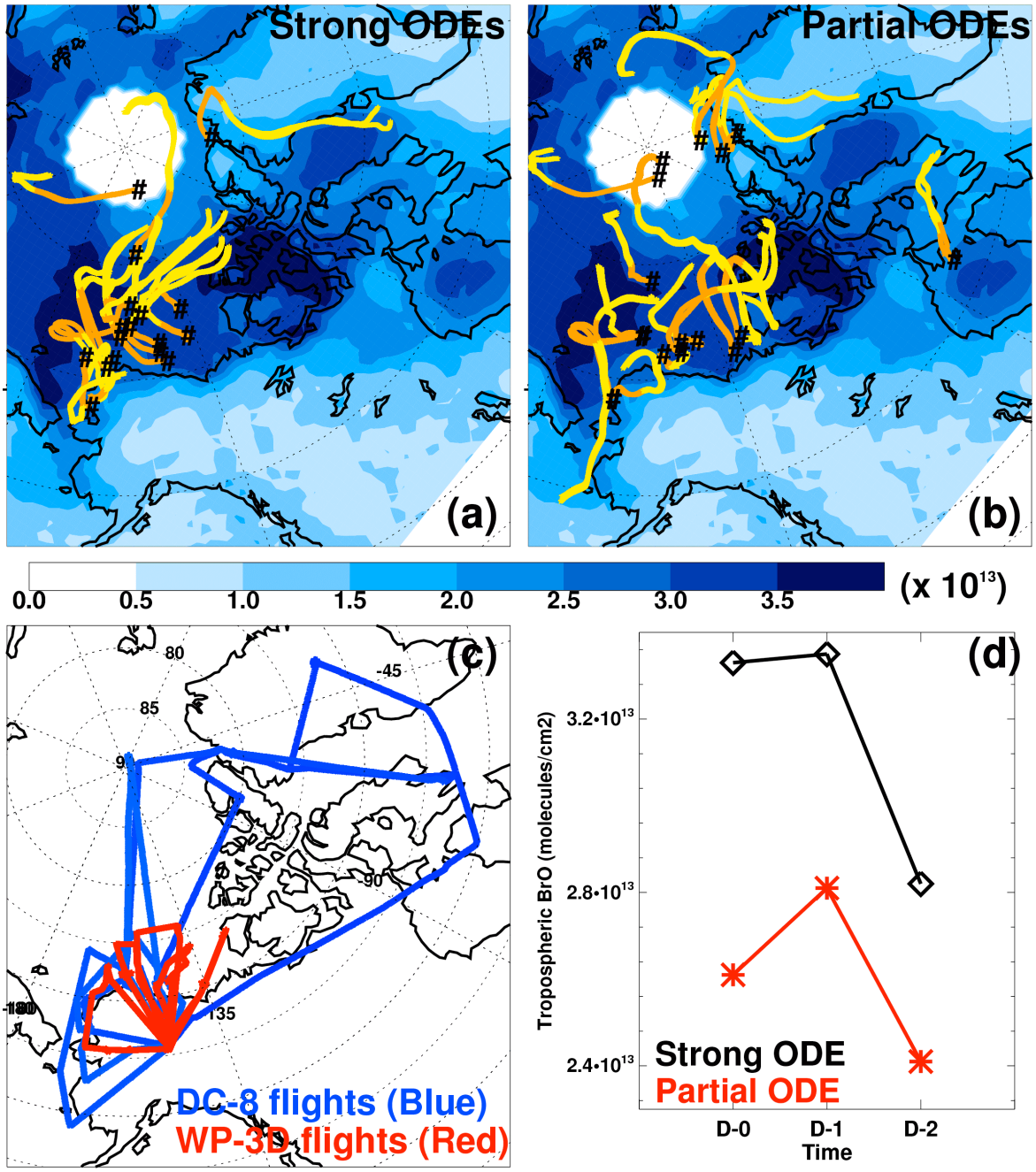

Fig. S14. Same as Fig. 5, but for tropospheric BrO VCDs of OMI-RAQMS.

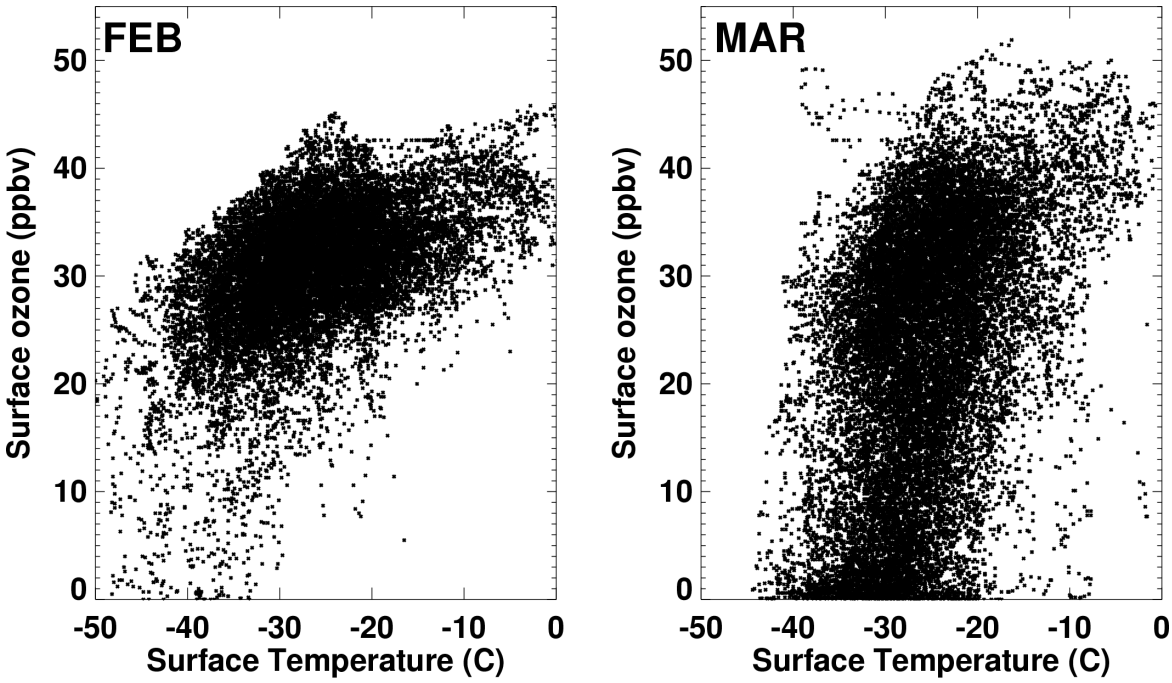

Fig. S15. Hourly surface ozone as a function of temperature at Barrow for February (left) and March (right). Ozone measurements from 1979 to 2008 were obtained from the NOAA Earth System Research Laboratory (ESRL) and the temperature dataset from the NOAA National Climate Data Center (NCDC).

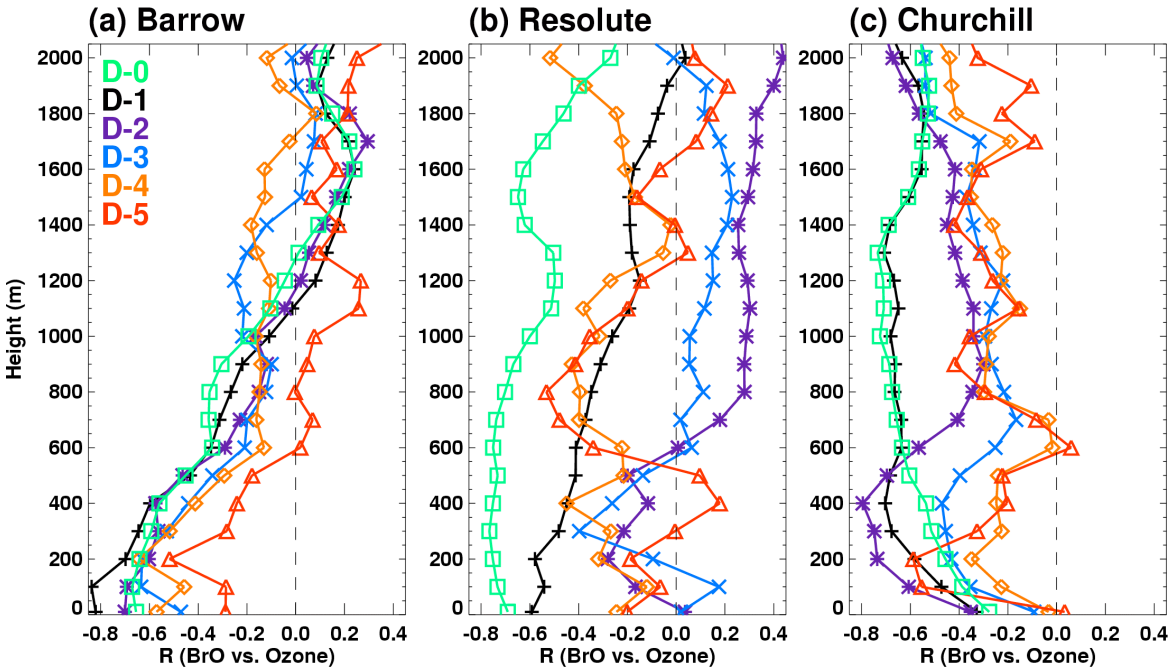

Fig. S16. Same as Fig. 9, but for tropospheric BrO VCDs of OMI-SCIA2ND.

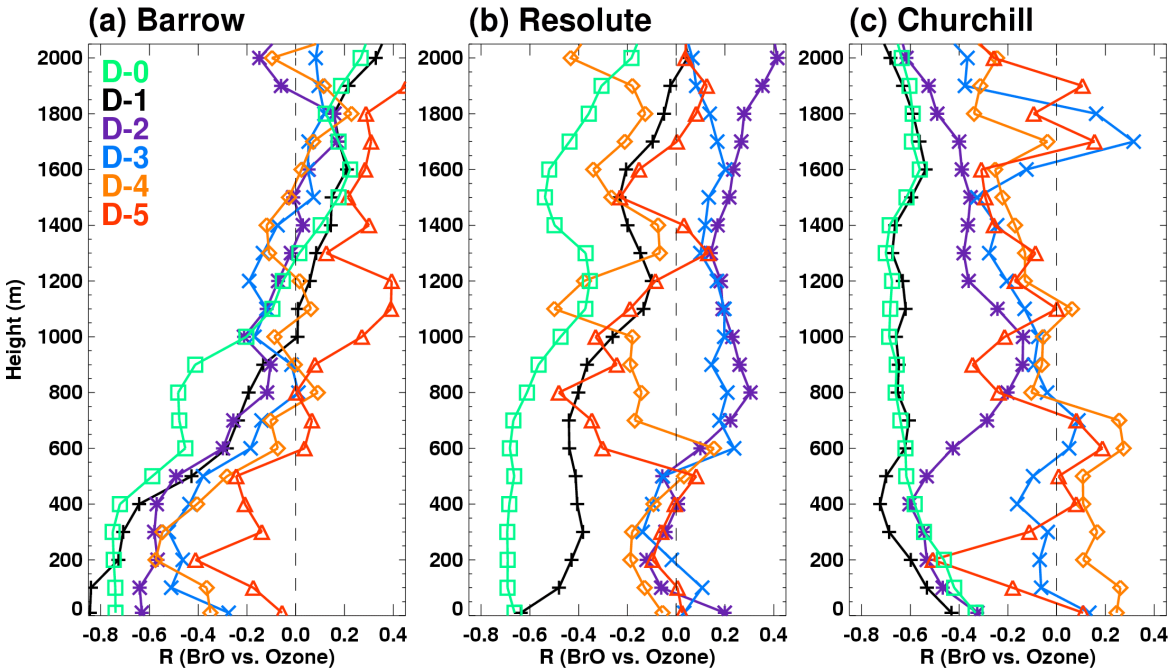

Fig. S17. Same as Fig. 9, but for tropospheric BrO VCDs of GOME2-20th.

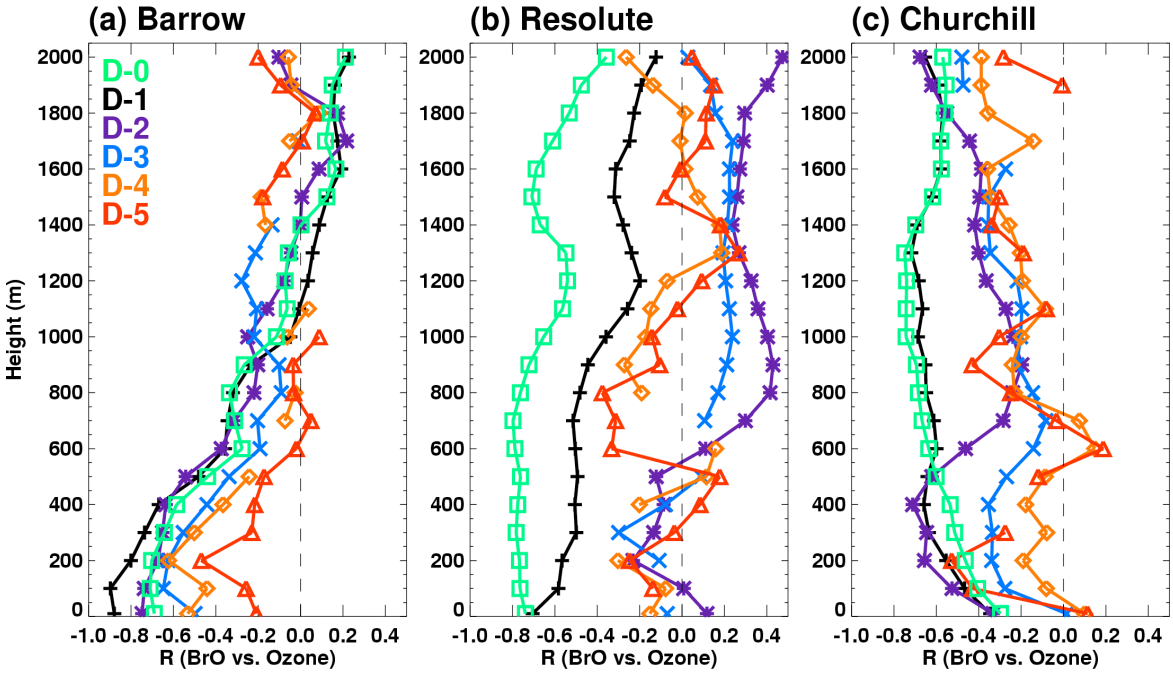

Fig. S18. Same as Fig. 9, but for tropospheric BrO VCDs of OMI-20th.

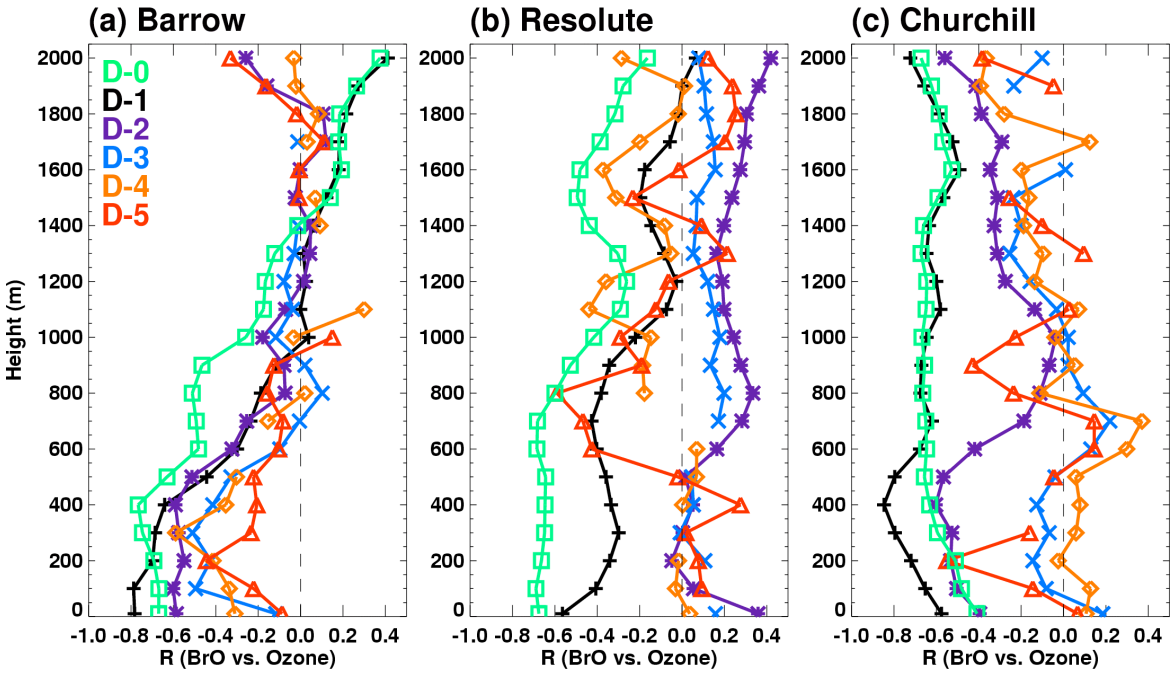

Fig. S19. Same as Fig. 9, but for tropospheric BrO VCDs of GOME2-RAQMS.

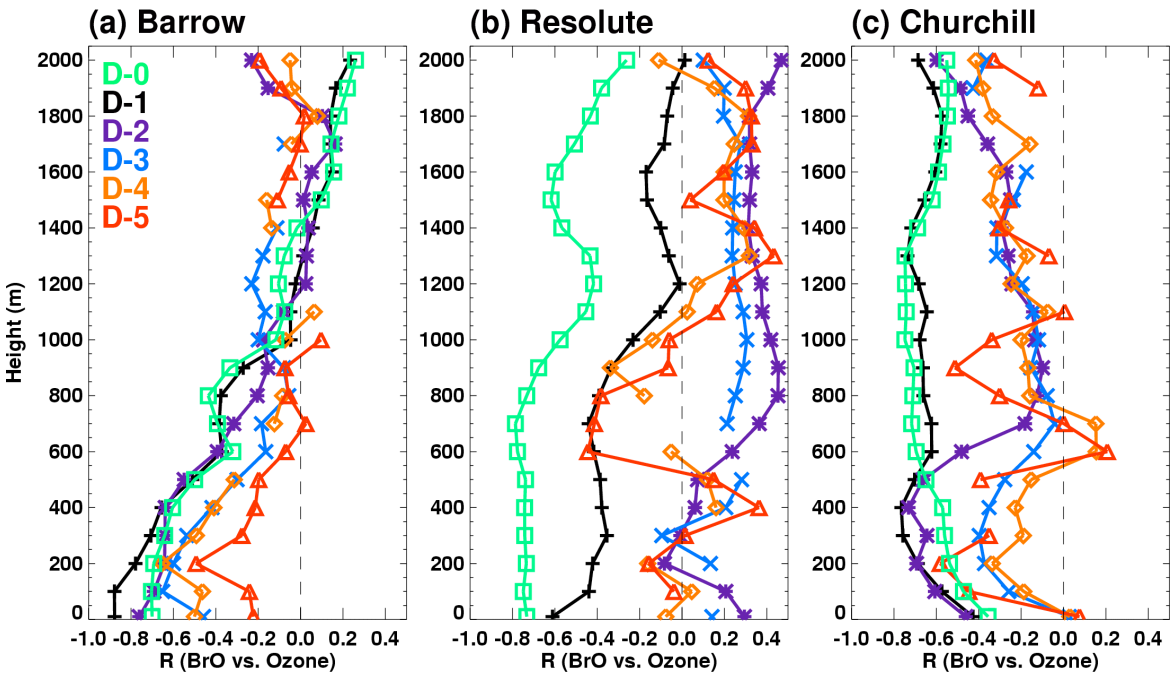

Fig. S20. Same as Fig. 9, but for tropospheric BrO VCDs of OMI-RAQMS.